Supplementary Materials

Atomically Dispersed Ru-Co Pairs on Hollow Carbon as Robust Catalysts for the Acidic Oxygen Evolution Reaction

Fengqin Zhang, Qingmei Wang[a]*, Zhijie Chen[b]*, Shun Lu[c]*

a School of Chemistry and Chemical Engineering, Guizhou University, Guiyang, Guizhou, 550025, China

b Water Research Centre, School of Civil and Environmental Engineering, The University of New South Wales, Sydney, NSW 2052, Australia

c Chongqing Institute of Green and Intelligent Technology, Chinese Academy of Sciences, Chongqing 400714, China

* Corresponding Authors: qmwang3@gzu.edu.cn (Q. Wang), zhijie.chen1@unsw.edu.au (Z. Chen), lushun@cigit.ac.cn (S. Lu)

Contents

Experimental details

Chemicals

Tetraethyl orthosilicate (TEOS, ≥98%), ammonia solution ($NH_3 \cdot H_2O$, 28-30%), ethanol (EtOH, 99.7%), dopamine hydrochloride (DA, ≥98%), sodium thiosulfate pentahydrate ($Na_2S_2O_3 \cdot 5H_2O$, ≥99%) as the sulfur source, cobalt nitrate hexahydrate ($Co(NO_3)_2 \cdot 6H_2O$, ≥98%), ruthenium(III) chloride hydrate ($RuCl_3 \cdot xH_2O$), hydrofluoric acid (HF, 10 wt% aq.). Commercial 20 wt% Pt/C, RuO_2, and 5 wt% Nafion solution were purchased from Sunlaite. Ultrapure water (18.2 MΩ·cm) was used throughout.

S-doped polydopamine-coated silica

Monodisperse SiO_2 spheres were prepared via a Stöber procedure. Distilled water (80 mL), EtOH (24 mL), and $NH_3 \cdot H_2O$ (1.0 mL, 28 wt%) were mixed at 25 °C for 20 min, followed by TEOS (1.0 mL, 4.48 mmol) and additional stirring for 20 min. DA (0.20 g, 1.05 mmol) and $Na_2S_2O_3 \cdot 5H_2O$ (0.13 g, 0.52 mmol; DA:S = 2:1 molar ratio) were then added to enable in situ SPDA deposition and S-doping. The mixture was stirred for 20 h at 25 °C. The product was collected by centrifugation (8000 rpm, 5 min, 3 cycles), washed with EtOH/water, and dried at 80 °C for 24 h to afford SiO_2@SPDA.

Preparation of RuCo/SNC

SiO_2@SPDA (0.20 g) was dispersed in water (50 mL) and EtOH (50 mL) by sonication for 15 min. A solution of $Co(NO_3)_2$ $6H_2O$ (1.5 mmol Co) and $RuCl_3$ xH_2O (nominally 1.5 mmol Ru) in 20 mL of water was added dropwise. The suspension was stirred for 20 h at 25 °C. The solid was collected by centrifugation (8000 rpm, 5 min), washed with EtOH, and dried to yield SiO_2@SPDA@Ru/Co. Carbonization was carried out in a quartz tube furnace under N_2: ramp 2 °C min^{-1} to 800 °C, hold 2 h, then cool naturally, affording SiO_2@SNC loaded with Ru/Co (SiO_2@SNC-RuCo).

Silica was removed by immersing the composite in 10 wt% HF (aq) at room temperature with a solid-liquid ratio of 10 mg mL^{-1} for 6 h under gentle stirring. The solid was washed with water to neutral pH and then EtOH and dried at 60 °C to give hollow RuCo/SNC.

In addition, Ru/SNC and Co/SNC were prepared identically to Section 2.3 using only $RuCl_3 \cdot xH_2O$ (1.5 mmol) or $Co(NO_3)_2 \cdot 6H_2O$ (1.5 mmol), respectively. Metal-free SNC was obtained by omitting metal salts.

Nominal composition and surface analysis

Nominal metal loadings and Ru/Co molar ratios were calculated from precursor amounts. Surface compositions and Ru/Co ratios were analyzed by XPS using charge-corrected spectra; elemental distributions were examined by Scanning transmission electron microscopy coupled with energy-dispersive X-ray spectroscopy (STEM-EDS) mapping when specified.

Physical Characterizations

The as-prepared RuCo/SNC catalyst was characterized and its phase identified using

X-ray diffraction (XRD) with a D8 DISCOVER instrument (Bruker AXS, Germany). Transmission electron microscopy (TEM) and high-resolution TEM (HRTEM) were performed to confirm the microstructure using a JEMARM200F microscope operated at 200 kV [1]. High-angle annular dark-field scanning transmission electron microscopy (HAADF-STEM) images were recorded with the same microscope at 300 kV. Energy dispersive X-ray spectroscopy (EDX) elemental mapping was conducted to analyze the distribution of different elements, with the spectrometer installed in the JEMARM200F and operated at 200 kV [2]. The X-ray photoelectron spectroscopy (XPS) analysis was performed using a K-Alpha Plus system (Somerfield, USA) with an Al-Ka X-ray source for illumination [3]. Inductively coupled plasma mass spectrometry (ICP-MS) analysis was manipulated on an Thermo ICAP PRO instrument. Additionally, the local electronic structure and coordination environment of the catalysts were examined by X-ray absorption near-edge structure (XANES) and extended X-ray absorption fine structure (EXAFS) at 300 K in PETRA III, beamline P64, of DESY, Germany. The Ru-K edge was measured by monitoring the incident and transmitted X-ray intensities using a gas ionization chamber in fluorescence and transmission modes. A monochromatic X-ray beam was obtained using Si (111) as the reflecting surface, and the energy was calibrated by defining the K-edge (first derivative maxima) energy of the copper foil as 8980.5 eV. Kirkpatrick-Baez (K-B) mirror optics were used to focus the X-ray beam. Rhodium-coated X-ray mirrors were used to suppress higher harmonics. A CCD detector was used to record the transmitted signals. X-ray absorption edge jumps with absorption coefficients varying close to the theoretical value of 1 were obtained by homogeneously mixing the samples with an inert cellulose matrix to prepare particles for XAFS analysis. ATHENA software was used to perform background subtraction, normalization and alignment of the EXAFS data. ARTEMIS software was used to construct the theoretical XAFS model and fit it to the experimental data to extract detailed information about the local structure of the samples.

To measure electrochemical capacitance, the cyclic voltammetry (CV) scans were performed 20 times between 0.20 and 0.30 V vs. RHE at each of the different scan rates (20, 40, 60, 80, and 100 mV/s). Capacitive currents were measured in a potential range where no faradic processes were observed [4]. The measured capacitive currents difference (ΔJ) was plotted as a function of scan rate and specific capacitances were determined from the slopes of the linear fitting. The specific capacitances were converted into an electrochemical surface area (ECSA) using the specific capacitance value for a flat standard with 1 cm^2 of real surface area [5].

Electrochemical measurements were carried out on a CHI 660E electrochemical analyzer (CH Instruments, Inc., Shanghai) using a standard three-electrode configuration. The electrolyte was 0.5 M H_2SO_4, which was thoroughly degassed by bubbling N_2 for at least 35 min prior to measurements to minimize interference from dissolved gases [6]. The as-prepared electrocatalyst was fabricated into an ink by dispersing 3 mg of catalyst in 500 μL ethanol with Nafion as the binder, and the resulting suspension was uniformly drop-cast onto a glassy carbon electrode for activity (performance) evaluation and onto carbon cloth for stability testing, with a

fixed catalyst loading of 0.3 mg cm^{-2} for both substrates. A carbon rod was used as the counter electrode, and a saturated Ag/AgCl electrode (in acidic electrolyte) served as the reference electrode. Prior to linear sweep voltammetry (LSV) measurements, the catalysts were electrochemically conditioned by cyclic voltammetry (CV) activation within 0.20-0.30 V (vs RHE) until a stable response was obtained, which helps remove surface contaminants and ensures a reproducible catalyst surface state. LSV polarization curves were then recorded in N_2-saturated electrolyte at a scan rate of 5 mV s^{-1}. Ohmic-drop correction was applied to all polarization data (iR compensation, partial compensation) to account for solution resistance losses; the solution resistance (Rs) was determined from the high-frequency intercept of the EIS Nyquist plot, and when applicable, impedance spectra were fitted using an equivalent circuit of Rs − (CPE ∥ Rct) to extract charge-transfer-related parameters[8-10]. All potential reported in this work were referenced to the reversible hydrogen electrode (RHE) using the relationship E (vs RHE) = E (vs Ag/AgCl) + 0.059 pH + 0.197 for a saturated Ag/AgCl reference electrode [11], ensuring consistent comparison across different conditions.

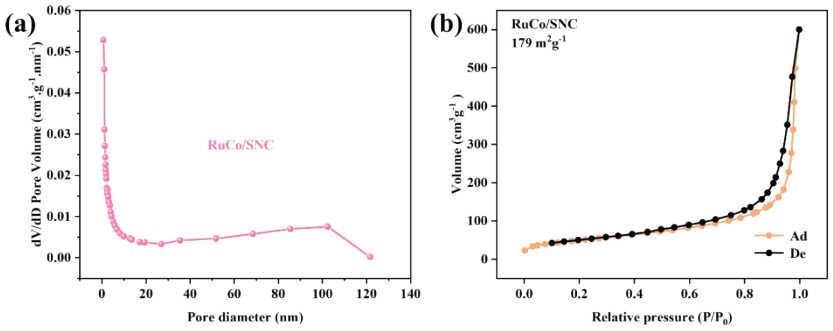

Figure S1. (a) Pore-size distribution, (b) N_2 adsorption-desorption isotherm of RuCo/SNC.

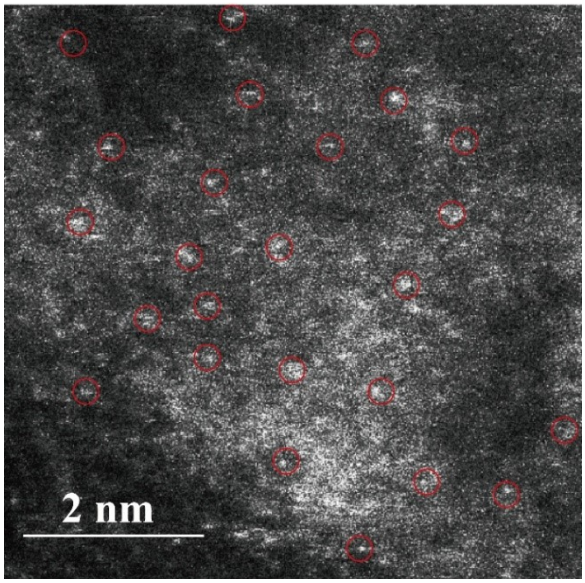

Figure S2. HAADF-STEM image of RuCo/SNC.

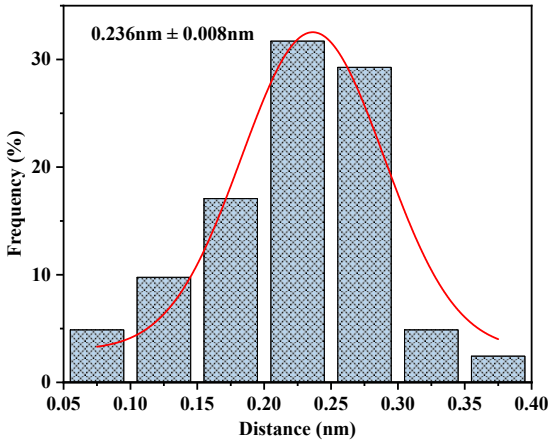

Figure S3. Statistical distance in the observed bimetal pairs.

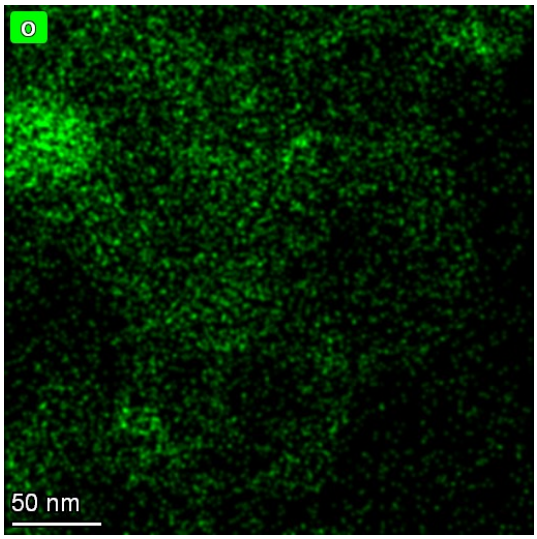

Figure S4. EDS mapping images of the O element in RuCo/SNC.

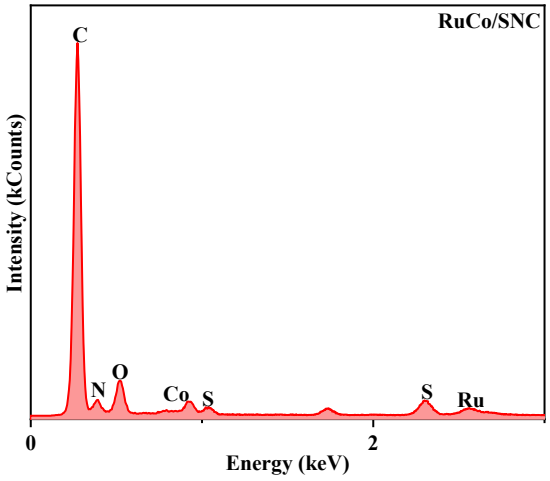

Figure S5. STEM-EDS spectrum of RuCo/SNC

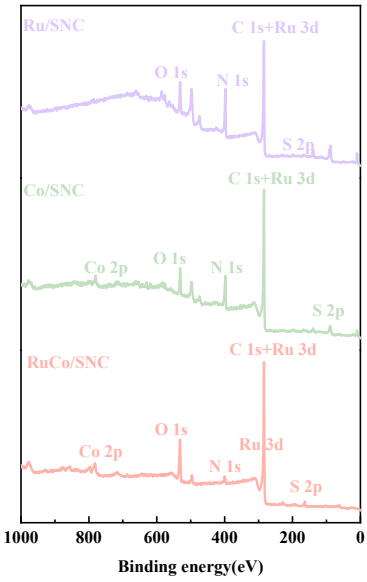

Figure S6. XPS survey spectra of Ru/SNC, Co/SNC, and RuCo/SNC.

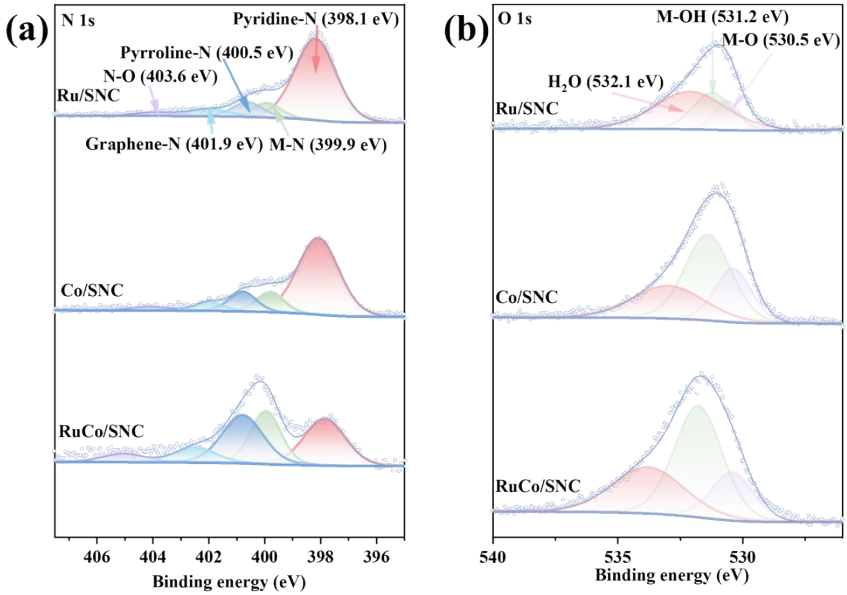

Figure S7. XPS spectra of Ru/SNC, Co/SNC and RuCo/SNC catalysts (a) N 1s, (b) O 1s.

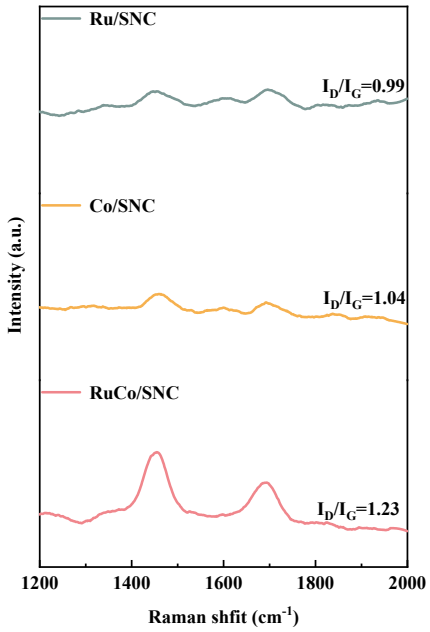

Figure S8. Raman spectra of RuCo/SNC catalysts.

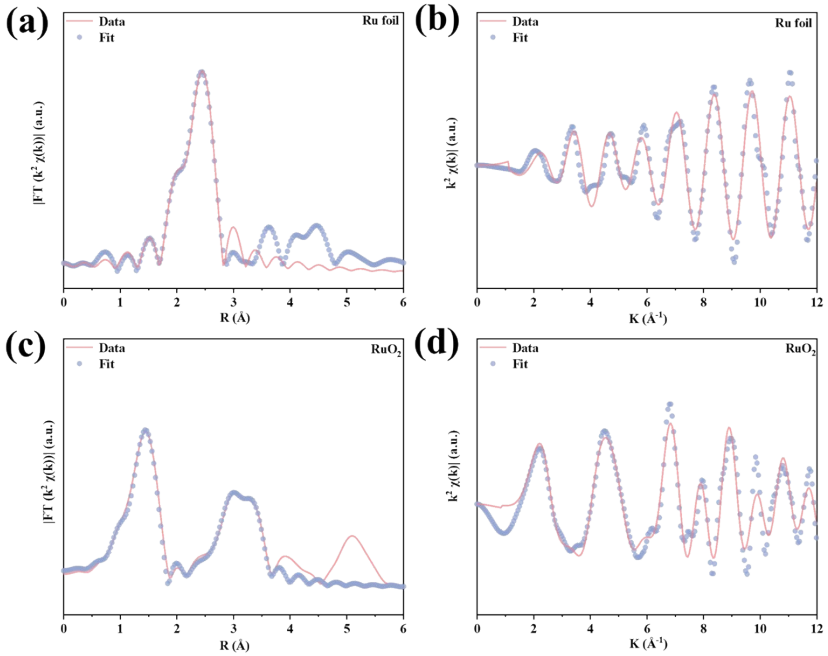

Figure S9. Ru K-edge EXAFS fitting results of reference samples. (a) Fourier-transformed Ru K-edge EXAFS spectra (k^2-weighted) of Ru foil in R space and the corresponding fitting curves (R-mag). (b) Ru K-edge EXAFS spectra of Ru foil in k space ($k^2\chi(k)$) with the corresponding fit. (c) Fourier-transformed Ru K-edge EXAFS spectra (k^2-weighted) of RuO_2 in R space and the corresponding fitting curves (R-mag). (d) Ru K-edge EXAFS spectra of RuO_2 in k space ($k^2\chi(k)$) with the corresponding fit.

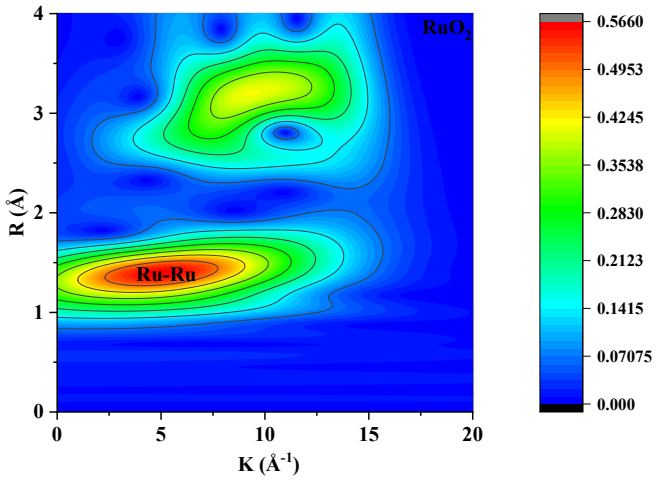

Figure S10. Ru K-edge WT-EXAFS contour map of RuO_2

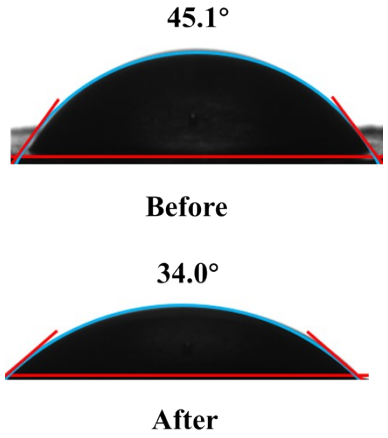

Figure S11. Contact angles of RuCo/SNC before and after etching.

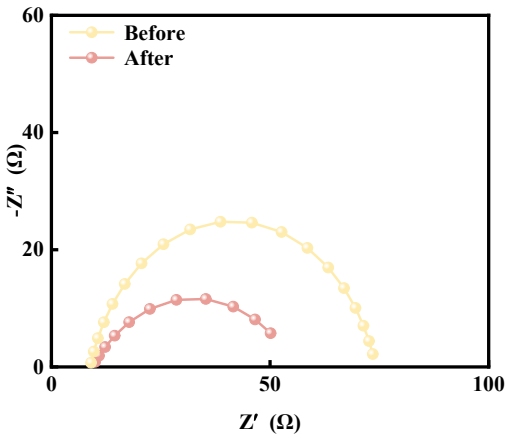

Figure S12. EIS of RuCo/SNC before and after etching.

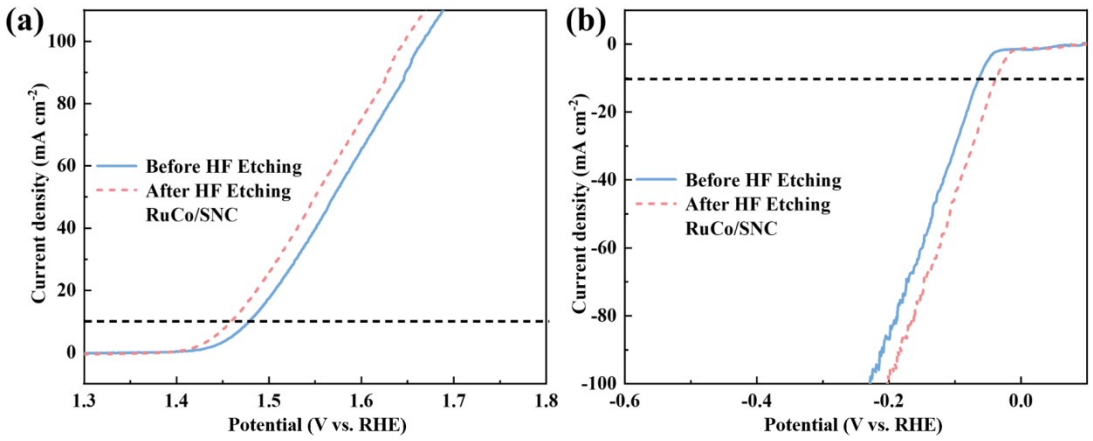

Figure S13. LSV of (a) OER and (b) HER for RuCo/SNC before and after etching.

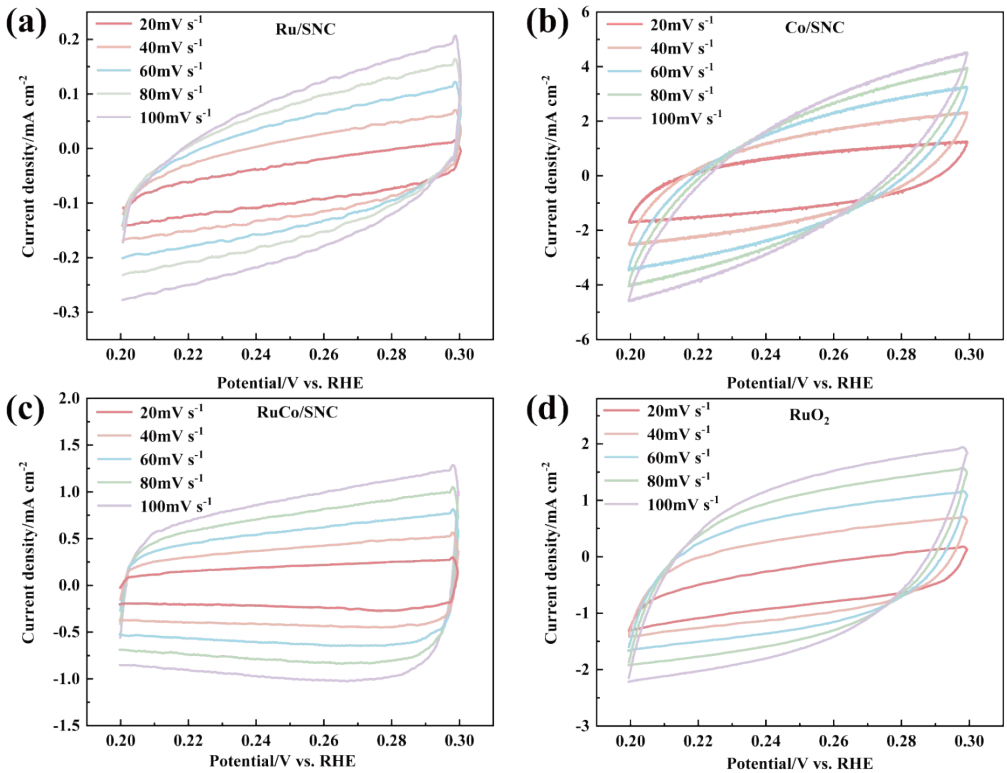

Figure S14. CV curves of (a)Ru/SNC, (b)Co/SNC, (c)RuO_2, (d)RuCo/SNC in H_2SO_4.

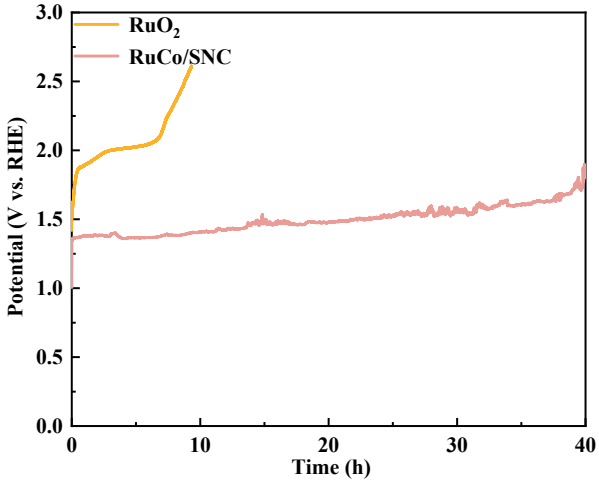

Figure S15. OER stability test (40 h).

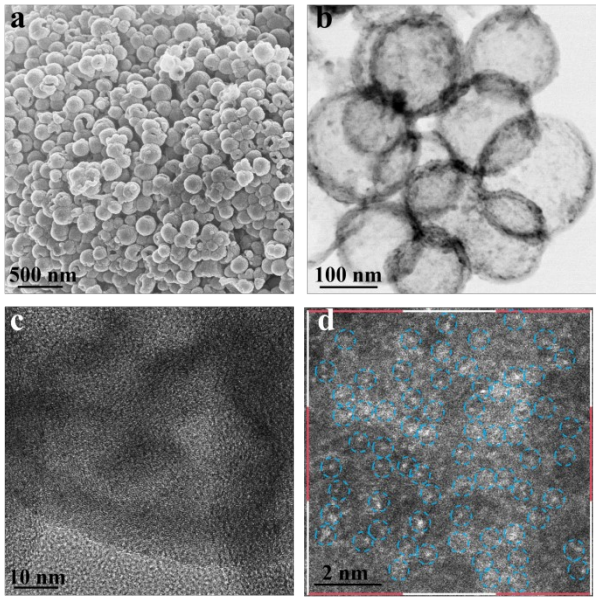

Figure S16. Post-OER characterizations of RuCo/SNC after 40h acidic OER test. (a) SEM, (b) TEM, (c) HRTEM, and (d) Aberration-corrected HAADF-STEM images.

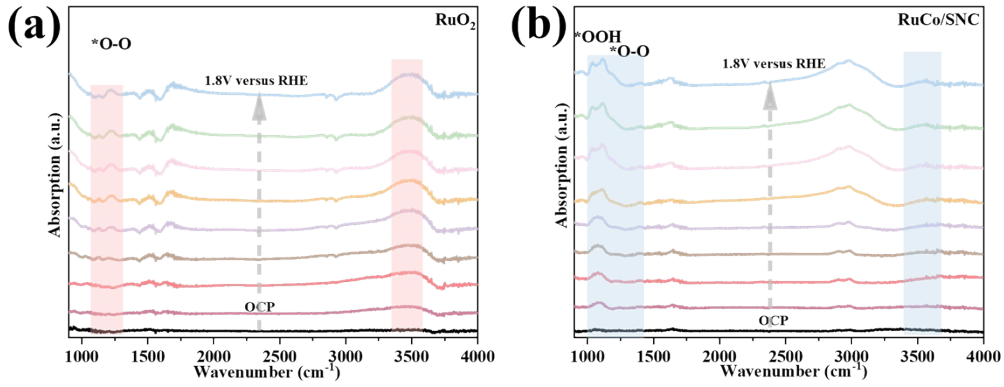

Figure S17. Stacked ATR-FTIR spectra recorded from OCP to 1.8 V vs. RHE of (a) RuO_2 and (b) RuCo/SNC.

Table S1. Ru, Co, C, N, O, and S of all samples were obtained from XPS analysis

Catalysts	Ru	Co	C	N	O	S
	Atomic (%)	Atomic (%)	Atomic (%)	Atomic (%)	Atomic (%)	Atomic (%)
RuCo/SNC	1.33	1.2	79.24	3.06	13.67	1.50
Ru/SNC	0.88	0	72.11	18.15	8.49	0.37
Co/SNC	0	0.53	78.24	14.14	6.62	0.47

Table S2. EXAFS fitting parameters at the Ru K-edge for various samples

Samples	Shell	CN[a]	R(Å)[b]	σ2(Å2)[c]	ΔE0(eV)[d]	R factor
Ru-foil	Ru-Ru	12*	2.672±0.003	0.0030	4.9±0.7	0.0053
	Ru-O	6.6±0.2	1.966±0.006	0.0025	-3.0±0.8	
RuO_2	Ru-Ru	9.8±0.9	3.143±0.010	0.0095	-5.3±1.0	0.0077
	Ru-Ru	5.8±0.4	3.584±0.007	0.0016	2.7±1.2	
	Ru-N	0.9±0.3	1.922±0.010	0.0011		
RuCo	Ru-S	1.1±0.2	2.297±0.017	0.0011	5.9±0.9	0.0060
	Ru-Ru	5.1±0.2	2.659±0.004	0.0005		

CN: coordination number; R: the distance to the neighboring atom; σ^2: the Mean Square Relative Displacement (MSRD); ΔE0: inner potential correction; R factor indicates the goodness of the fit. $S0^2$ was fixed to 0.7, according to the experimental EXAFS fit of Ru foil by fixing CN as the known crystallographic value.

Table S3. Metal dissolution after 40 h OER in acidic electrolyte (ICP-MS, μg L^{-1}).

Catalysts	Ru	Co
RuCo/SNC	2.3	6.1
Ru/SNC	13.2	0
Co/SNC	0	7.9
RuO_2	22.6	0

References

[1] Muthurasu A, Maruthapandian V, Kim HY. Metal-organic framework derived Co_3O_4/MoS_2 heterostructure for efficient bifunctional electrocatalysts for oxygen evolution reaction and hydrogen evolution reaction. Appl Catal B: Environ 2019; 248: 202-10.

[2] Chen Z, Gong W, Wang J, Hou S, Yang G, Zhu C, et al. Metallic W/WO_2 solid-acid catalyst boosts hydrogen evolution reaction in alkaline electrolyte. Nat Commun 2023; 14: 5363.

[3] Saleem A, Chen J, Liu M, Liu N, Usman M, Wang K, et al. Versatile Magnetic Mesoporous Carbon Derived Nano-Adsorbent for Synchronized Toxic Metal Removal and Bacterial Disinfection from Water Matrices. Small 2023; 19: e2207348.

[4] Pu Z, Zhao J, Amiinu IS, Li W, Wang M, He D, et al. A universal synthesis strategy for P-rich noble metal diphosphide-based electrocatalysts for the hydrogen evolution reaction. Energy Environ Sci 2019; 12: 952-7.

[5] Yuan C, Cheng G, Ruan W, Ma B, Yuan X, Zhang X, et al. Efficient hydrogen production in an innovative S-doped CoMoO4-based electrolytic cell: 12.97% less energy consumption. Sustain Mater Techno 2023; 37.

[6] Li S, Cheng C, Sagaltchik A, Pachfule P, Zhao C, Thomas A. Metal-organic precursor–derived mesoporous carbon spheres with homogeneously distributed molybdenum carbide/nitride nanoparticles for efficient hydrogen evolution in alkaline media. Adv Funct Mater 2018; 29.

[7] Risch M. Reporting activities for the oxygen evolution reaction. Commun Chem 2023; 6: 221.
[8] McCrory CCL, Jung S, Peters JC, Jaramillo TF. Benchmarking heterogeneous electrocatalysts for the oxygen evolution reaction. J Am Chem Soc 2013; 135(45): 16977-87.
[9] Zlatar M, Escalera-López D, Gamón Rodríguez M, et al. Standardizing OER electrocatalyst benchmarking in aqueous electrolytes: comprehensive guidelines for accelerated stress tests and backing electrodes. ACS Catal 2023; 13(23): 15375-92.
[10] Wu C, Tang Y, Zou A, et al. Recommended electrochemical measurement protocol for oxygen evolution reaction. DeCarbon 2025; 8: 100108.
[11] Zang W, Sun T, Yang T, Xi S, Waqar M, Kou Z, et al. Efficient hydrogen evolution of oxidized Ni-N_3 defective sites for alkaline freshwater and seawater electrolysis. Adv Mater 2021; 33: e2003846.